Supporting information

for

Synthesis, structural characterisation, and anticancer potential of mono and dinuclear Pd(II) complexes of N-(2-pyridyl)thiourea

Shivendra Kumar Pandey[a†], Sandeep Kumar[b†], Swati Singh[a], Anand Kumar Patel [b], Mannu Kumar Gond [a], Arbind Acharya[b], Manoj Kumar Bharty[a*]

[a] Department of Chemistry, Banaras Hindu University, Varanasi-221005, India.

[b] Department of Zoology, Banaras Hindu University, Varanasi-221005, India.

*Corresponding author E-Mail: mkbharty@bhu.ac.in

†Authors contributed equally in this work

1. Materials

Reagents Methylisothiocynate (TCI Chemicals), 3-Methyl-2-aminopyridine (Avra Chemicals, India), Palladium dichloride (Sigma-Aldrich), KCl (Rankem Chemicals) were procured from commercial sources and used without purification. The experiments were conducted under ambient conditions. The solvents used were purchased from Merck and were purified before use as per the standard procedure.

2. Physical measurements

Infrared Spectra were recorded in the 400-4000 cm^{-1} region as KBr pellets on a PerkinElmer Spectrum two. ^{1}H and ^{13}C NMR spectra were noted in DMSO-D_6 on a JEOL JNM-ECZ500R/S1 FT-NMR spectrometer using TMS as an internal reference. Electronic spectra were recorded at 10^{-5} M solution in DMSO on a SHIMADZU 1700 UV-Vis spectrophotometer. Electrospray Ionization Mass Spectrometric (ESI-MS) measurements have been attained from SCI-EX X500R QTOF high resolution mass spectrometer.

3. Crystal structure determination

The crystal data was gathered using a graphite mono-chromated Cu/Mo Kα(λ=1.54841/0.71073Å) radiation source at 293K on an Oxford Gemini diffractometer using CryAlis CCD software. The structures were solved using by Direct methods (SHELXL-18) through a multiscan absorption correction, and full-matrix least squares on F^2 were utilized to refine the results against all data using anisotropic displacement parameters for all atoms apart from hydrogen in Olex 2.0.[1-3] All hydrogen atoms were included in the refinement at a geometrically ideal position and refined with a riding model. The MERCURY package for Windows program were used for generating structures.[4]

4. Solution Stability

Assessing the stability of complexes in water is crucial for determining the biological effectiveness of any metallodrug. A stock solution of 10^{-3} M of each complex was prepared in DMSO (to improve solubility). The sample solutions were prepared to 10^{-5} M by taking 30 µL of stock diluting with 2970 µL of phosphate-buffered saline (PBS) and then the stability of complexes (10^{-5} M) was carried out. The absorption spectra of the complexes were measured with increasing time 0h, 2h, 4h, 6h, 12h, 18h, 24h and 48h at room temperature.[5]

Further, stability is investigated with ^{1}H NMR. ^{1}H NMR spectra of complexes is recorded over a period of 72 hrs in the presence of water.

5. Evaluation of anticancer activity

Cell Culture and maintenance

The Human colon cancer (HT-29), Breast cancer (MCF-7) and normal human embryonic kidney (HEK-293) cell lines were procured from the NCCS, Pune, India and were maintained in the cell culture flask containing Dulbecco Modified Eagle Medium (DMEM) with L-glutamine which was supplemented with penicillin, streptomycin and 10% FBS. Cells were maintained in a humidified atmosphere containing 5% CO2 at 37˚ C. The cells were harvested when they reached 80–90% confluence and plated for subsequent experiments.

Assessment of cytotoxicity by MTT Assay

Evaluation of cytotoxicity was assessed using MTT (3-(4,5-dimethylthiazol-2-yl)-2,5 diphenyltetrazolium bromide dye) assay in HT-29 and MCF-7 cells. Breifly 1×10^4 cells/well of HT-29, MCF-7 and HEK-293 cell lines were seeded in 96 well flat bottom plates supplemented with DMEM medium (10% FBS and antibiotic solution) and incubated to adhere overnight under humidified CO_2 incubator. After incubation period media was discarded and cells were then treated for 24 h with different concentrations of ligand, palladium complex and cisplatin, used as a positive control. Following incubation, drug containing media was removed and then 100 μL MTT (5 mg/mL in PBS) was added to each well and incubated for additional 2 h to allow formazan crystal formation. Formed crystals were dissolved in 100 µL DMSO and absorbance was measured at 595 nm using an ELISA plate reader (Bio-Rad, CA, USA).[6] Cell viability was calculated relative to the untreated control group using the following equation:

$$\%\ Cell\ Viability = \frac{[Absorbance\ in\ the\ treated\ group]}{[Absorbance\ in\ the\ untreated\ group]} \times\ 100$$

Acridine orange/propidium iodide (AO/EB) dual staining

The morphological changes in HT-29 cells after treatment with **[Pd(M3MPyThU)Cl]$_2$** was identified qualitatively using AO/EtBr staining. For this study briefly 1×10^5 cells/well in 6 well culture plate were treated with varying concentrations (5, 10 and 20 µM) of **[Pd(M3MPyThU)Cl]$_2$** for a duration of 24 h at a temperature of 37 ℃ and a CO_2 level of 5%. The cells were washed after treatment and fixed with 4% paraformaldehyde solution for 8-10 min and subsequently permeabilized by 0.1% TritonX100 followed by staining with 20 µM of AO/EtBr solution and incubated for

15 min in dark. Finally, cells were then observed by fluorescent microscope (Nikkon E 800, Japan) at 40X magnification[7].

Estimation for intracellular ROS generation

The ability of **[Pd(M3MPyThU)Cl]$_2$** to induce reactive oxygen species (ROS) production in HT-29 cancer cells was assessed using confocal microscopy. The levels of oxidative stress and reactive oxygen species (ROS) in cancer cells are significantly elevated compared to normal cells, primarily because of aberrant metabolism. To investigate the likely cause of apoptotic induction, the redox state was evaluated using DCFH-DA dye following the established protocol[8]. This is because intracellular ROS can play a significant role in the induction of apoptosis. HT-29 cells were placed in 6 well tissue culture plates and exposed to several concentrations (5, 10, and 20 μM) of **[Pd(M3MPyThU)Cl]$_2$**. Following the incubation period, the cells were rinsed two times with PBS and then treated with a 20 μM solution of DCFH-DA dye at a temperature of 37 °C for a duration of 30 min. The fluorescent intensity of stained cells was visualized under a confocal microscope (LSM-780, ZEISS) at 20X magnification for qualitative assessment.

Measurement of mitochondrial membrane potential (ΔΨm) by Rh-123

To evaluate the impact of **[Pd(M3MPyThU)Cl]$_2$** on mitochondrial-dependent apoptosis, we assessed mitochondrial membrane potential (ΔΨm) using Rh-123 staining. Rh-123 is a fluorescent dye that accumulates in mitochondria in a potential-dependent manner. A decrease in Rh-123 fluorescence intensity indicates mitochondrial depolarization, a hallmark of apoptosis[9]. Briefly, HT-29 cells (1 x 10^5 cells/well) were seeded in 96-well plates and treated with **[Pd(M3MPyThU)Cl]$_2$** at various concentrations (5, 10, and 20 μM) for 24 h under standard culture conditions (37 °C, 5% CO_2). Following incubation, cells were washed with PBS, stained with Rh-123 for 30 min at room temperature, and then analyzed for fluorescence intensity using confocal microscopy (LSM-780, ZEISS) at 20X magnification.

Statistical analysis

A comparison between the groups was conducted using either an unpaired student's t-test or a two-way ANOVA, followed by Bonferroni posttests. The experiment was conducted in triplicate and the data was reported as the average value plus or minus the standard deviation (SD). Differences were considered significant for p-value < 0.05. *<0.05, **<0.01 and ***<0.001.

6. I.R. Spectra of ligand and complexes

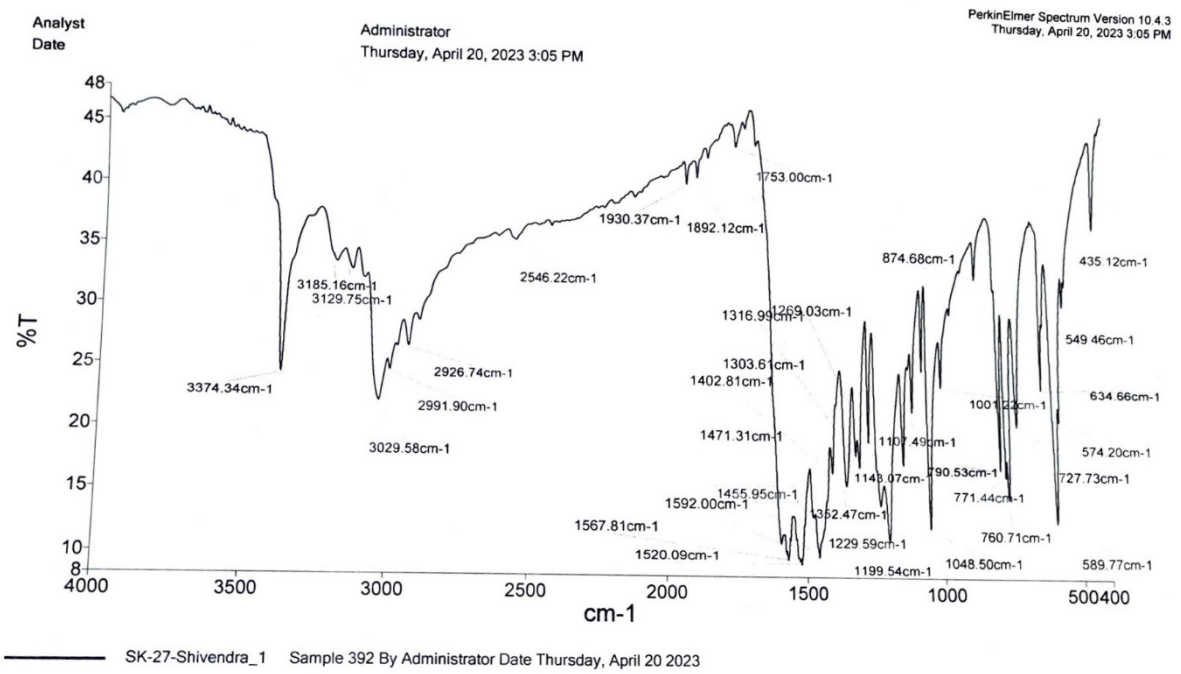

Supporting Fig. S1: IR spectrum of **HM3MPyThU**

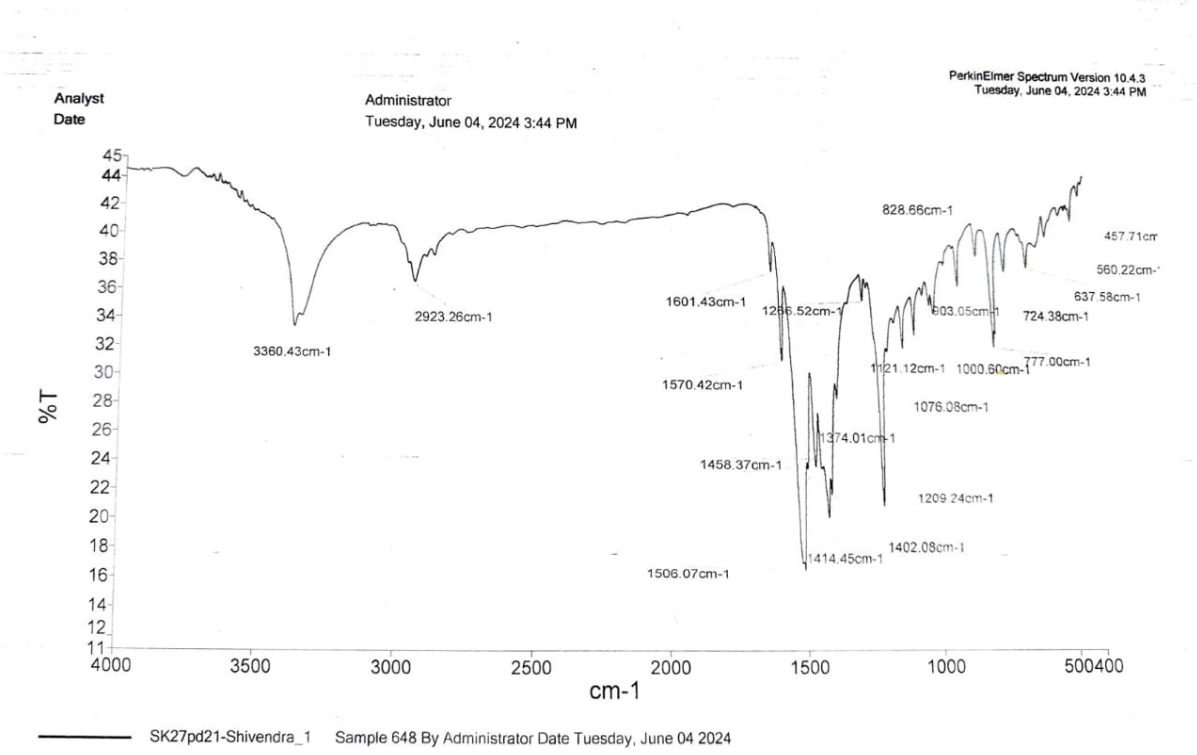

Supporting Fig. S2: IR spectrum of **[Pd(M3MPyThU)$_2$]**

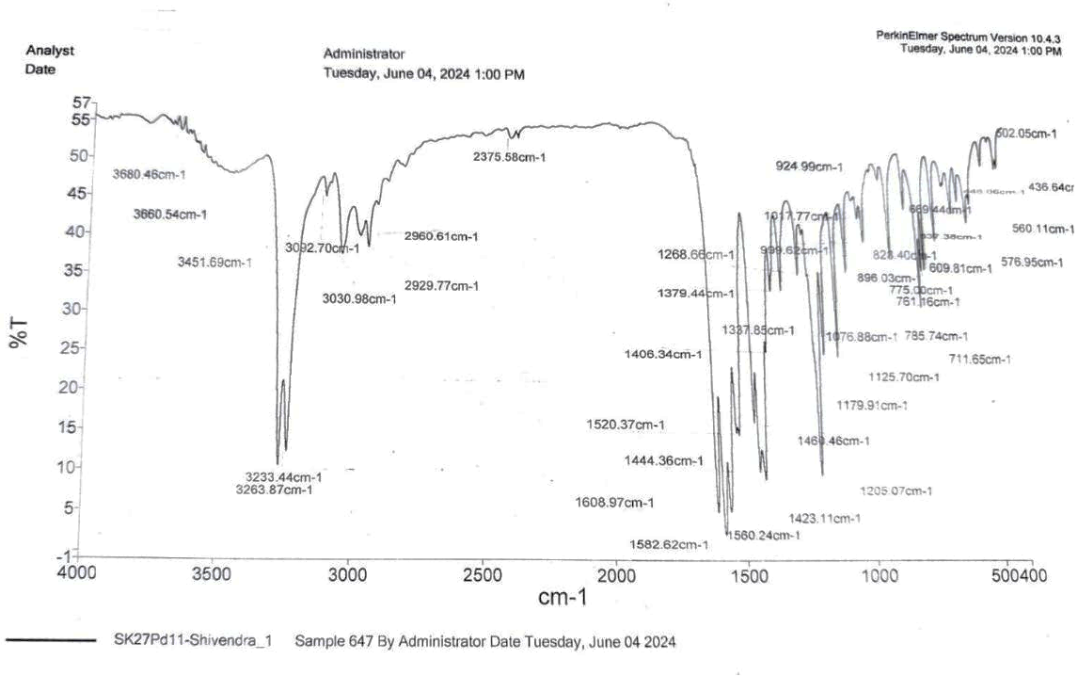

Supporting Fig. S3: IR spectrum of **[Pd(M3MPyThU)Cl]$_2$**

7. NMR spectra of ligand and complexes

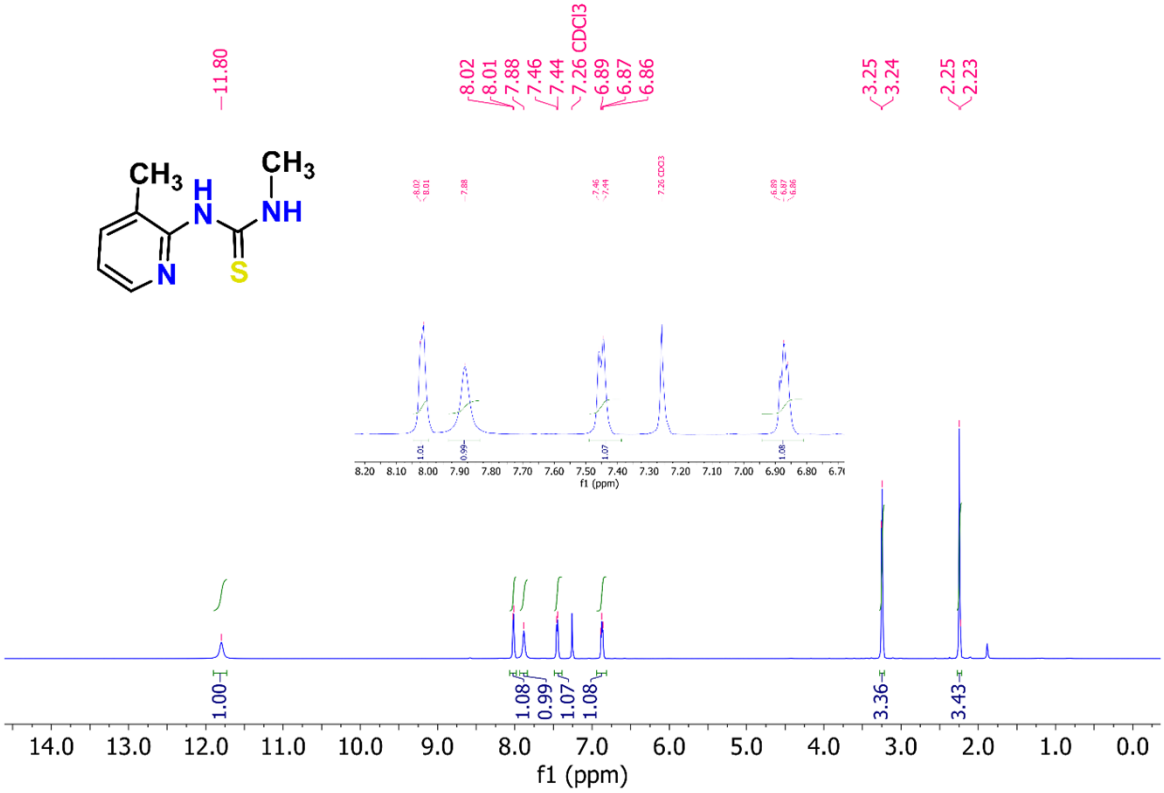

Supporting Fig. S4: ^{1}H NMR spectrum of **HM3MPyThU** in $CDCl_3$

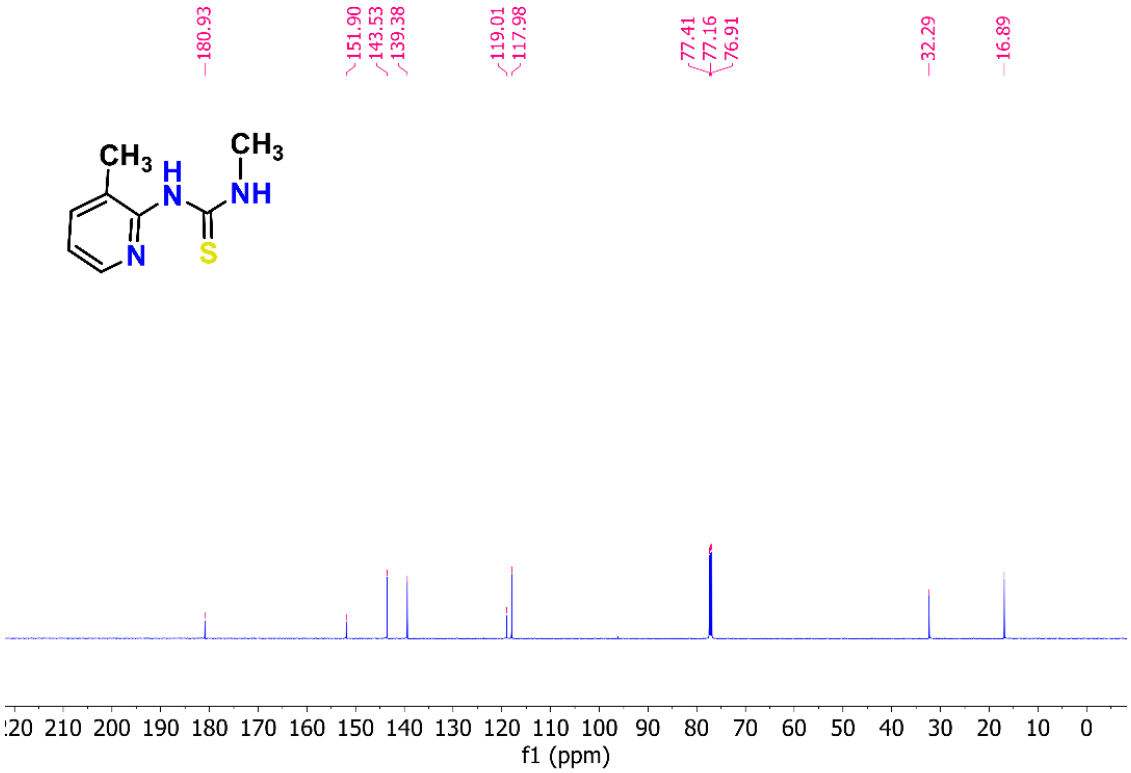

Supporting Fig. S5: ^{13}C NMR spectrum of **HM3MPyThU** in $CDCl_3$

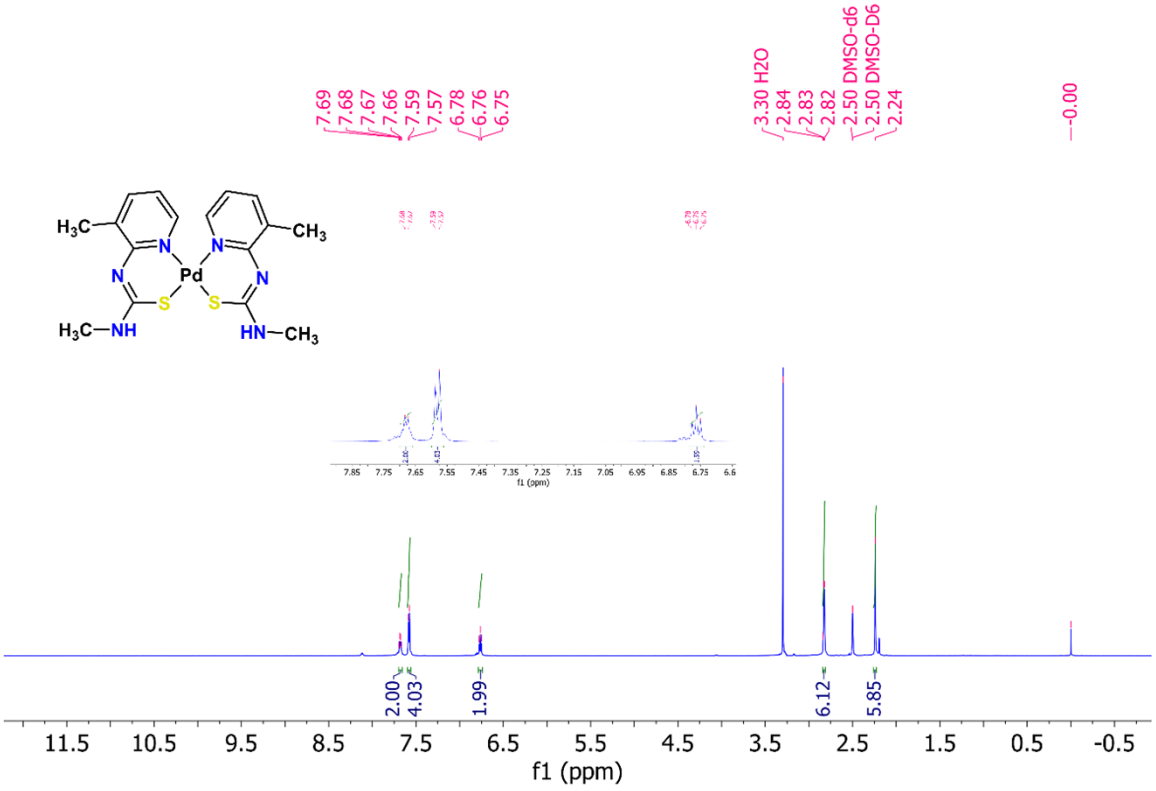

Supporting Fig. S6: ^{1}H NMR spectrum of **[Pd(M3MPyThU)$_2$]** in DMSO-d_6

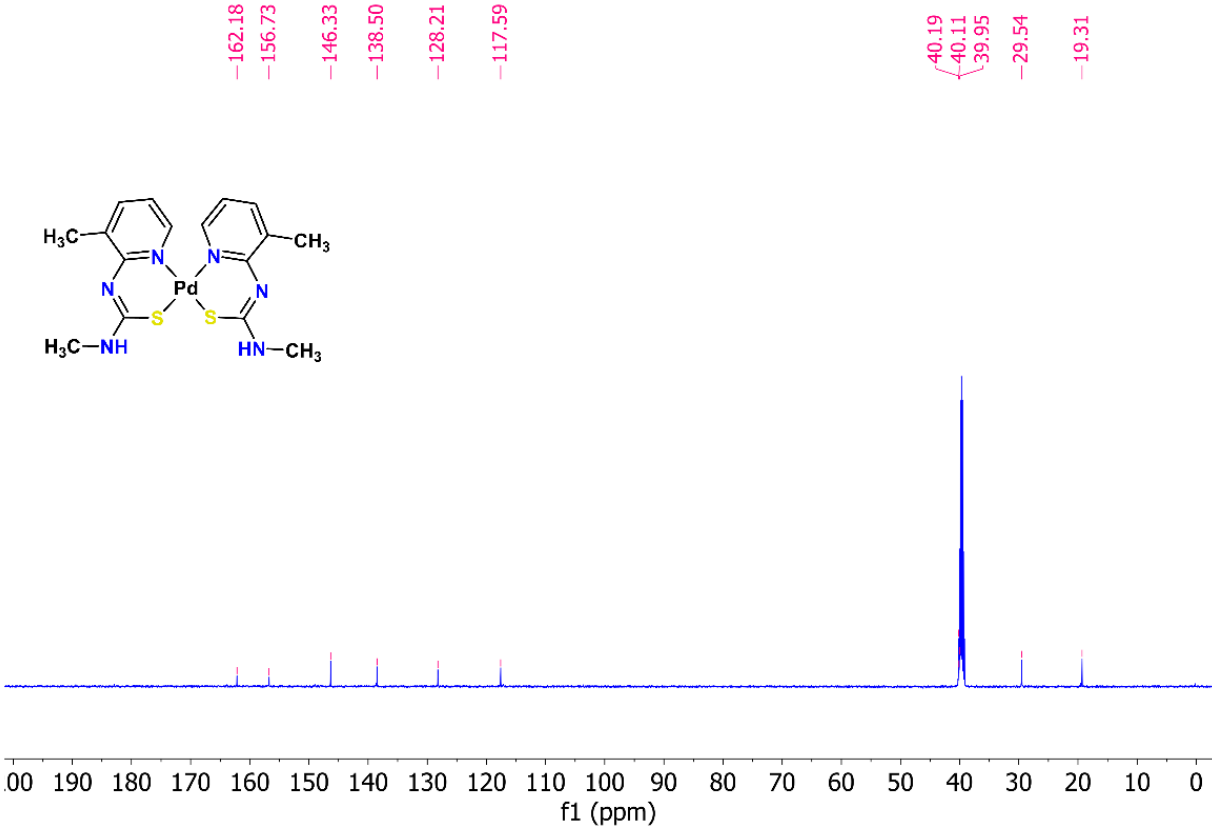

Supporting Fig. S7: ^{13}C NMR spectrum of **[Pd(M3MPyThU)$_2$]** in DMSO-d_6

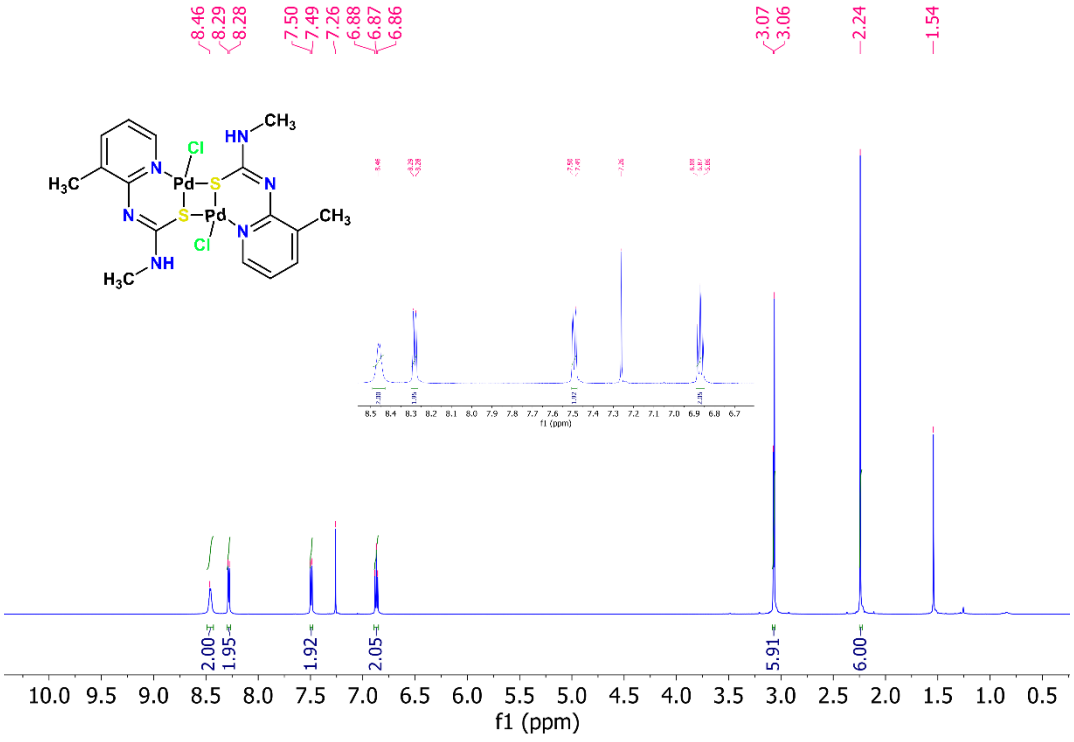

Supporting Fig. S8: ^{1}H NMR spectrum of **[Pd(M3MPyThU)Cl]$_2$** in $CDCl_3$

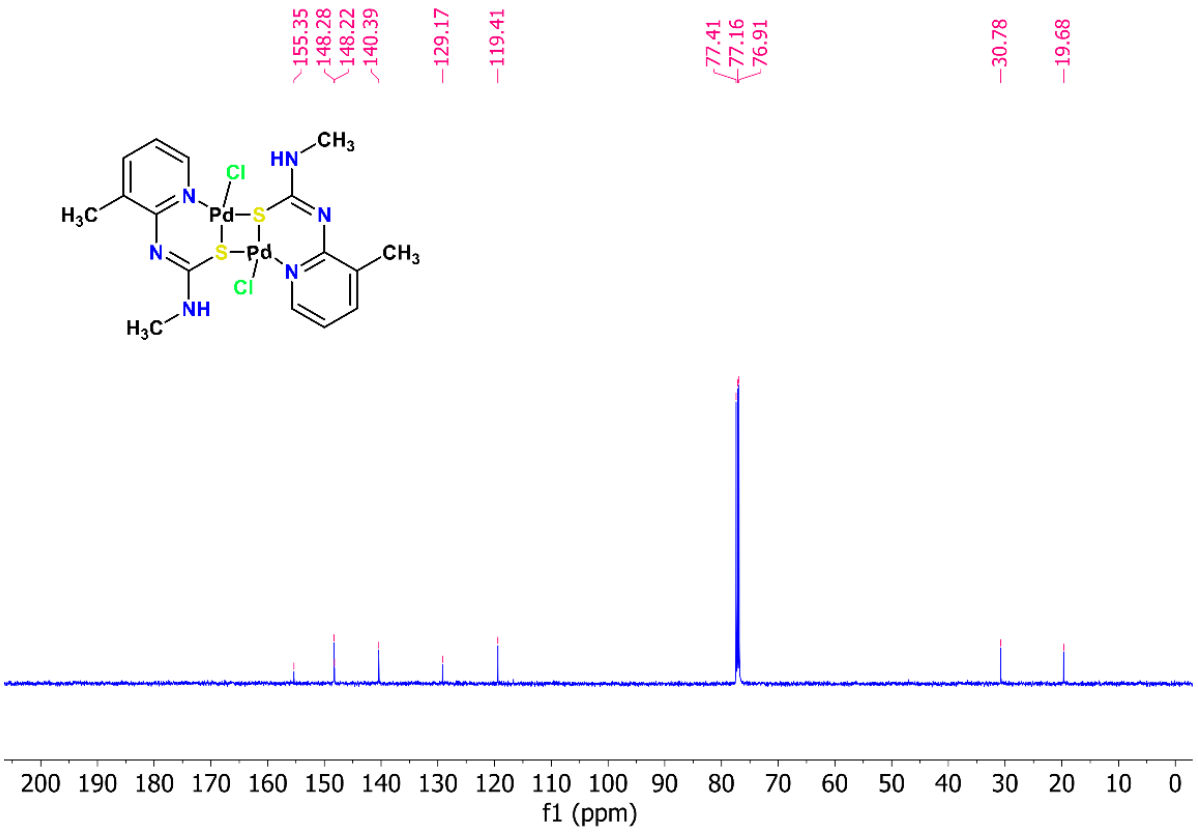

Supporting Fig. S9: ^{13}C NMR spectrum of **[Pd(M3MPyThU)Cl]$_2$** in $CDCl_3$

8. HRMS figures

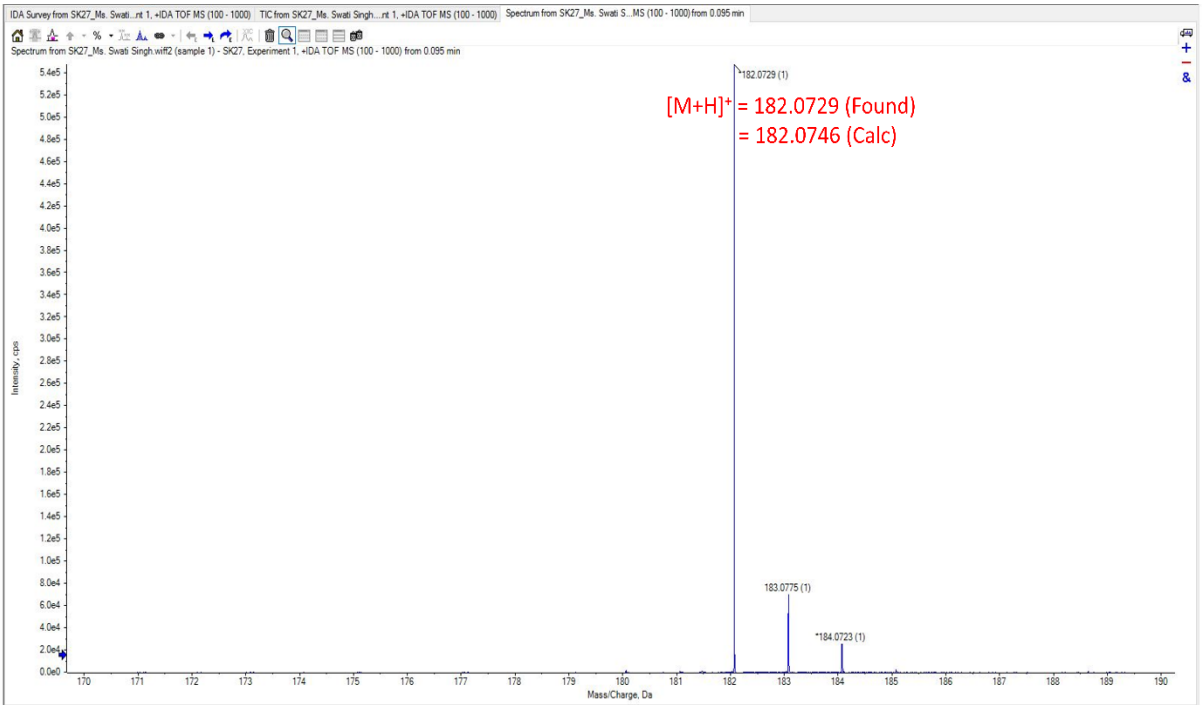

Supporting Fig. S10: HRMS spectrum of **HM3MPyThU**

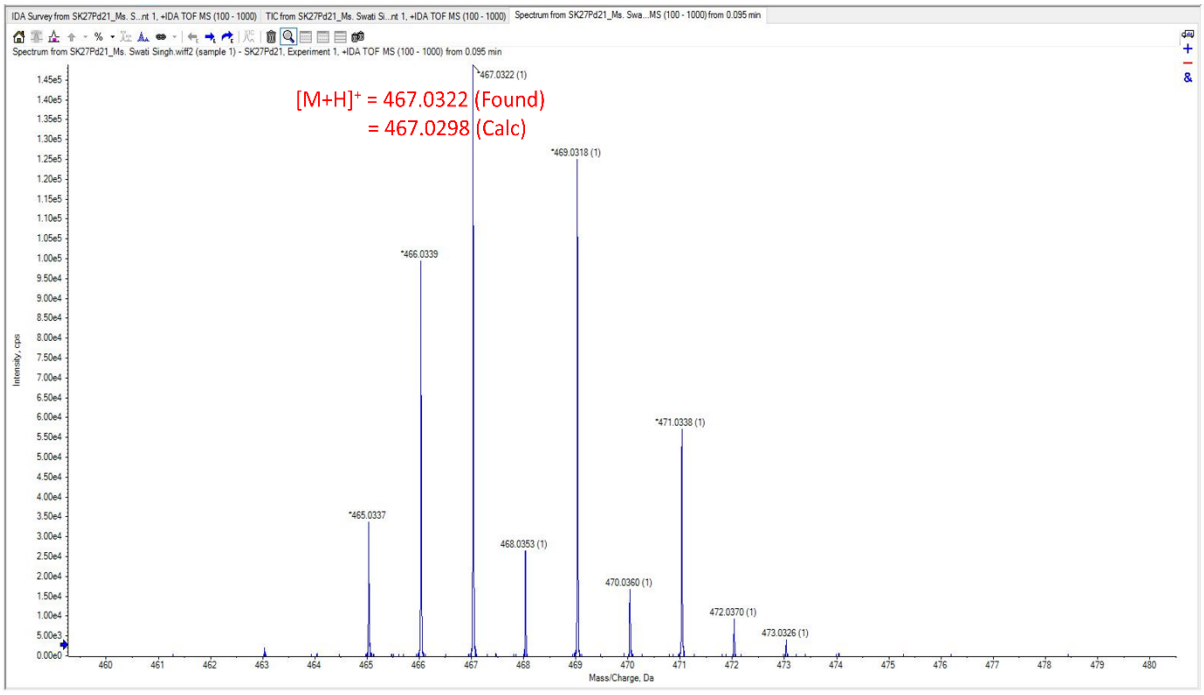

Supporting Fig. S11: HRMS spectrum of **[Pd(M3MPyThU)$_2$]**

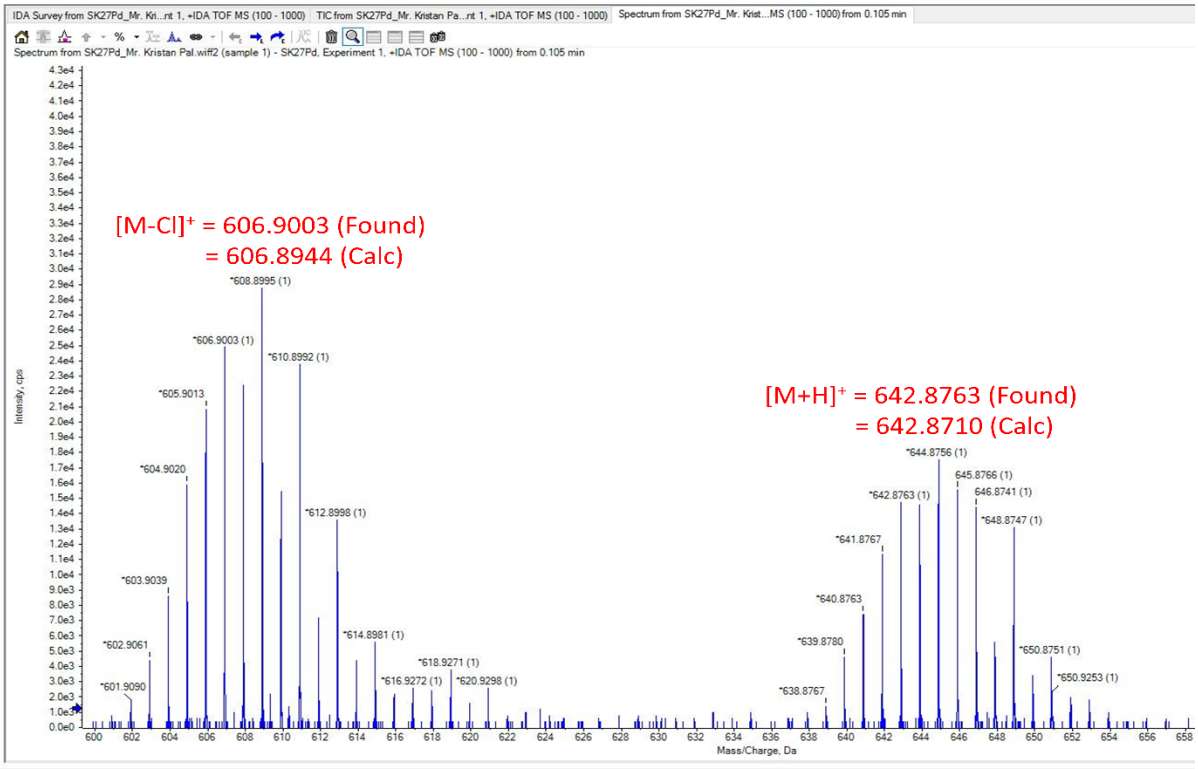

Supporting Fig. S12: HRMS spectrum of **[Pd(M3MPyThU)Cl]$_2$**

9. Crystallographic tables and figures

Supporting Table 1: Selected interatomic distances and angles for **HM3MPyThU**

Bond length (Å)		Bond angle (º)	
S(1)-C(7)	1.687(4)	**C(7)-N(2)-C(6)**	130.7(4)
N(2)-C(7)	1.377(5)	**C(6)-N(1)-C(1)**	117.6(3)
N(2)-C(6)	1.393(5)	**C(7)-N(3)-C(8)**	123.5(4)
N(1)-C(6)	1.327(5)	**C(3)-C(4)-C(6)**	116.5(3)
N(1)-C(1)	1.341(5)	**C(3)-C(4)-C(5)**	121.8(3)
N(3)-C(7)	1.317(6)	**N(1)-C(6)-N(2)**	118.1(3)
N(3)-C(8)	1.459(5)	**N(1)-C(6)-C(4)**	123.1(4)
C(4)-C(3)	1.375(5)	**N(2)-C(6)-C(4)**	118.7(3)
C(4)-C(6)	1.412(5)	**N(3)-C(7)-N(2)**	117.1(4)
C(4)-C(5)	1.506(5)	**N(3)-C(7)-S(1)**	124.5(3)
C(3)-C(2)	1.382(6)	**N(2)-C(7)-S(1)**	118.3(3)
C(1)-C(2)	1.359(6)	**N(1)-C(1)-C(2)**	124.1(4)

Supporting Table 2: Inter and intramolecular interactions [Å and º] for **HM3MPyThU**

D-H···A	d(D-H)	d(H···A)	d(D···A)	<(DHA)
N(3)-H(3)···N(1)	0.86	1.97	2.660(5)	136.6
C(2)-H(2A)···S(1)#1	0.93	3.01	3.695(4)	131.7

Symmetry transformations used to generate equivalent atoms: #1 x+1,y,z

Supporting Table 3: Selected interatomic distances and angles for **[Pd(M3MPyThU)$_2$]**

Bond length (Å)		Bond angle (º)	
Pd(1)-N(4)	2.064(7)	**N(4)-Pd(1)-N(1)**	93.9(2)
Pd(1)-N(1)	2.077(6)	**N(1)-Pd(1)-S(1)**	90.22(17)
Pd(1)-S(1)	2.2610(18)	**N(4)-Pd(1)-S(2)**	88.78(18)
Pd(1)-S(2)	2.2642(17)	**S(1)-Pd(1)-S(2)**	87.61(6)
S(1)-C(7)	1.759(7)	**C(7)-S(1)-Pd(1)**	102.3(3)
S(2)-C(15)	1.771(8)	**C(15)-S(2)-Pd(1)**	99.4(2)
N(5)-C(15)	1.305(10)	**C(15)-N(5)-C(14)**	124.8(6)
N(2)-C(6)	1.370(10)	**C(1)-N(1)-Pd(1)**	115.8(5)
N(2)-C(7)	1.304(11)	**C(6)-N(1)-Pd(1)**	125.5(5)
N(2)-C(6)	1.371(9)	**N(5)-C(15)-N(6)**	117.8(7)
N(1)-C(1)	1.350(9)	**N(5)-C(15)-S(2)**	128.6(6)

N(1)-C(6)	1.366(9)	**N(6)-C(15)-S(2)**	113.6(6)
C(15)-N(6)	1.337(10)	**C(11)-C(12)-C(14)**	119.0(6)

Supporting Table 4: Inter and intramolecular interactions [Å and º] for **[Pd(M3MPyThU)$_2$]**

D-H···A	d(D-H)	d(H···A)	d(D···A)	<(DHA)
N(3)-H(3)···N(2)#1	0.86	2.41	3.012(11)	127.3
C(1)-H(1)···N(4)	0.93	2.70	3.157(9)	111.3
C(8)-H(8A)···S(1)#2	0.96	2.88	3.668(9)	140.3
C(8)-H(8C)···N(2)#1	0.96	2.70	3.293(13)	120.6
N(6)-H(6)···S(2)#3	0.86	2.65	3.444(7)	154.5

Symmetry transformations used to generate equivalent atoms:

#1 -x, y-1/2, -z+2 #2 -x, y+1/2, -z+2 #3 -x, y-1/2, -z+1

Supporting Table 5: Selected interatomic distances and angles for **[Pd(M3MPyThU)Cl]$_2$**

Bond length (Å)		Bond angle (º)	
Pd(2)-N(4)	2.062(3)	**N(4)-Pd(2)-S(2)**	90.29(8)
Pd(2)-S(2)	2.2710(8)	**N(4)-Pd(2)-S(1)**	173.69(8)
Pd(2)-S(1)	2.3003(8)	**S(2)-Pd(2)-S(1)**	83.46(3)
Pd(2)-Cl(2)	2.3375(9)	**N(4)-Pd(2)-Cl(2)**	94.14(8)
Pd(1)-N(1)	2.063(3)	**S(2)-Pd(2)-Cl(2)**	175.28(3)
Pd(1)-S(1)	2.2771(8)	**S(1)-Pd(2)-Cl(2)**	92.14(3)
Pd(1)-S(2)	2.3223(8)	**N(1)-Pd(1)-S(1)**	88.08(9)
Pd(1)-Cl(1)	2.3316(10)	**N(1)-Pd(1)-S(2)**	170.12(9)
S(1)-C(7)	1.809(4)	**S(1)-Pd(1)-S(2)**	82.83(3)
S(2)-C(15)	1.804(4)	**N(1)-Pd(1)-Cl(1)**	92.24(9)
N(4)-C(14)	1.358(5)	**S(1)-Pd(1)-Cl(1)**	176.83(4)
N(4)-C(9)	1.361(5)	**S(2)-Pd(1)-Cl(1)**	97.05(3)
N(1)-C(1)	1.353(5)	**C(7)-S(1)-Pd(1)**	92.51(11)
N(1)-C(6)	1.355(5)	**C(7)-S(1)-Pd(2)**	108.47(11)
N(5)-C(15)	1.292(5)	**Pd(1)-S(1)-Pd(2)**	94.08(3)
N(5)-C(14)	1.370(5)	**C(15)-S(2)-Pd(2)**	97.85(12)
N(2)-C(7)	1.284(5)	**C(15)-S(2)-Pd(1)**	111.07(12)
N(2)-C(6)	1.378(5)	**Pd(2)-S(2)-Pd(1)**	93.65(3)
N(6)-C(15)	1.331(5)	**C(14)-N(4)-C(9)**	119.2(3)

N(6)-C(16)	1.452(5)	**C(14)-N(4)-Pd(2)**	122.8(2)
N(3)-C(7)	1.328(5)	**C(9)-N(4)-Pd(2)**	117.9(3)
N(3)-C(8)	1.448(5)	**C(1)-N(1)-C(6)**	119.8(3)

Supporting Table 6: Inter and intramolecular interactions [Å and º] for **[Pd(M3MPyThU)Cl]$_2$**

D-H···A	d(D-H)	d(H···A)	d(D···A)	<(DHA)
N(6)-H(6)···Cl(1)	0.86	2.32	3.162(3)	166.8
N(3)-H(3)···Cl(2)	0.86	2.43	3.221(3)	153.2
C(1)-H(1)···Cl(1)	0.93	2.80	3.279(4)	113.1
C(9)-H(9)···S(1)#1	0.93	2.93	3.414(4)	113.6
C(9)-H(9)···Cl(2)	0.93	2.77	3.281(4)	115.8
C(10)-H(10)···Cl(2)#2	0.93	2.96	3.716(4)	139.5

Symmetry transformations used to generate equivalent atoms:

#1 -x+1,-y+1,-z+1 #2 -x+2,-y+1,-z+1

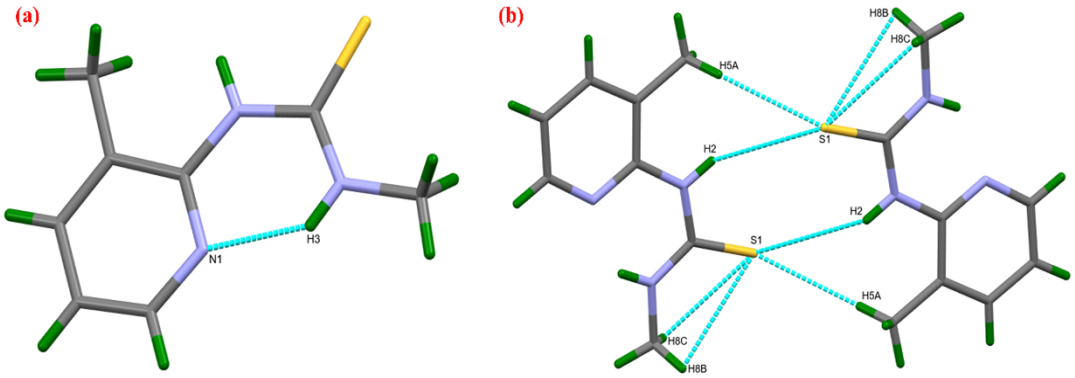

Supporting Fig. S13: Showing intramolecular (a) N-H···N and (b) intramolecular N-H···S and intermolecular C-H···S hydrogen bonding interactions in **HM3MPyThU** leading to flower-like architectures.

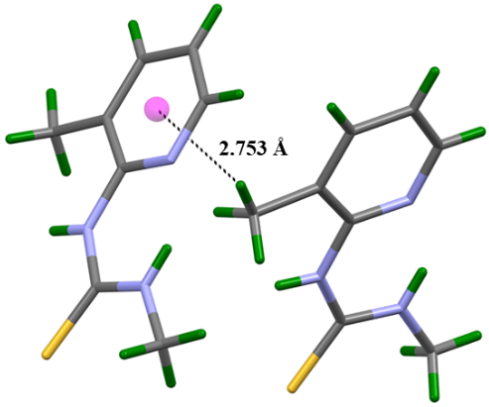

Supporting Fig. S14: Showing intermolecular C-H···π interactions in **HM3MPyThU**

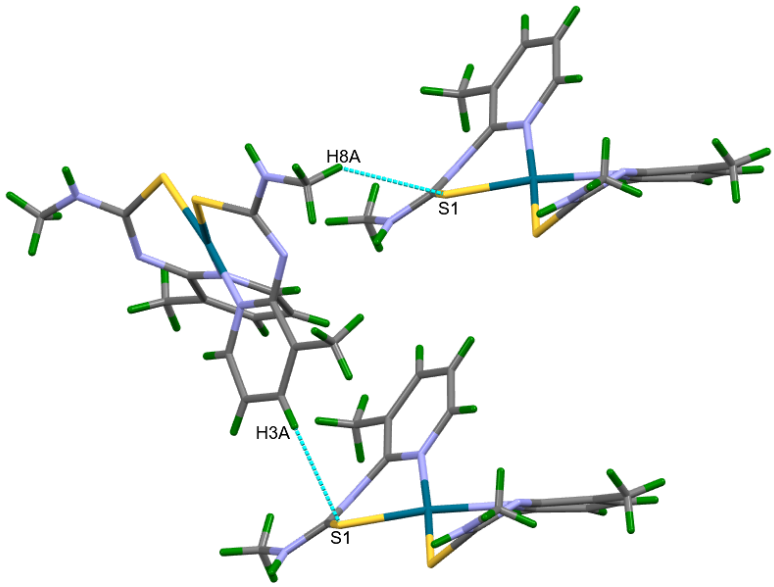

Supporting Fig. S15: Showing intermolecular C-H···S hydrogen bonding interactions in **[Pd(M3MPyThU)$_2$]**.

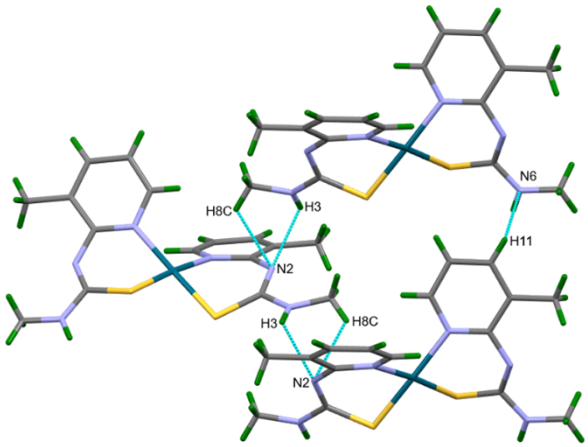

Supporting Fig. S16: Showing intermolecular C-H···N and N-H···N hydrogen bonding interactions in **[Pd(M3MPyThU)$_2$]**.

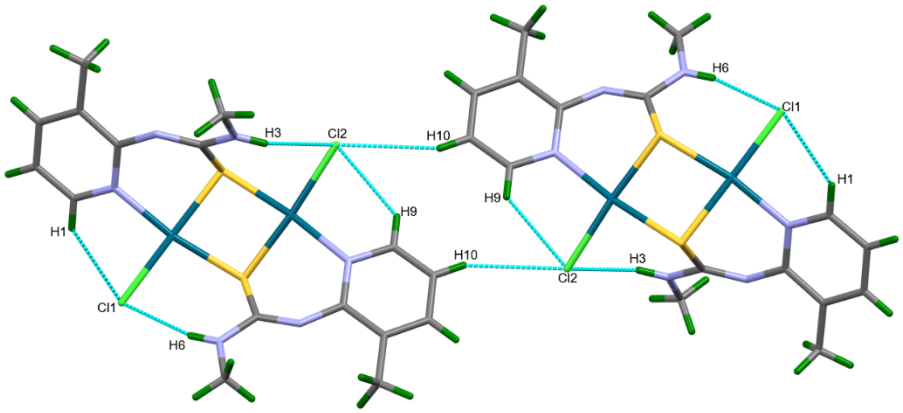

Supporting Fig. S17: Showing inter and intra molecular C-H···Cl hydrogen bonding interactions in **[Pd(M3MPyThU)Cl]$_2$**

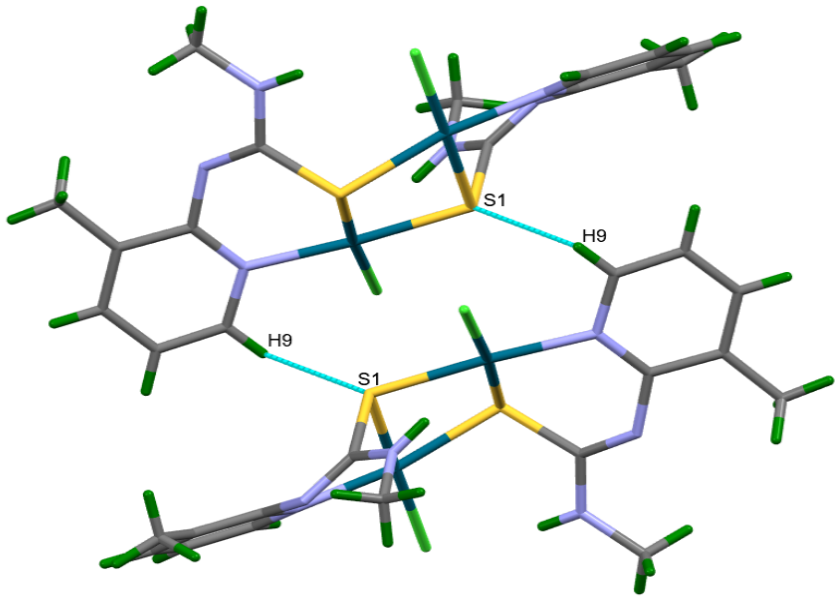

Supporting Fig. S18: Showing intermolecular C-H···S hydrogen bonding interactions in **[Pd(M3MPyThU)Cl]$_2$**

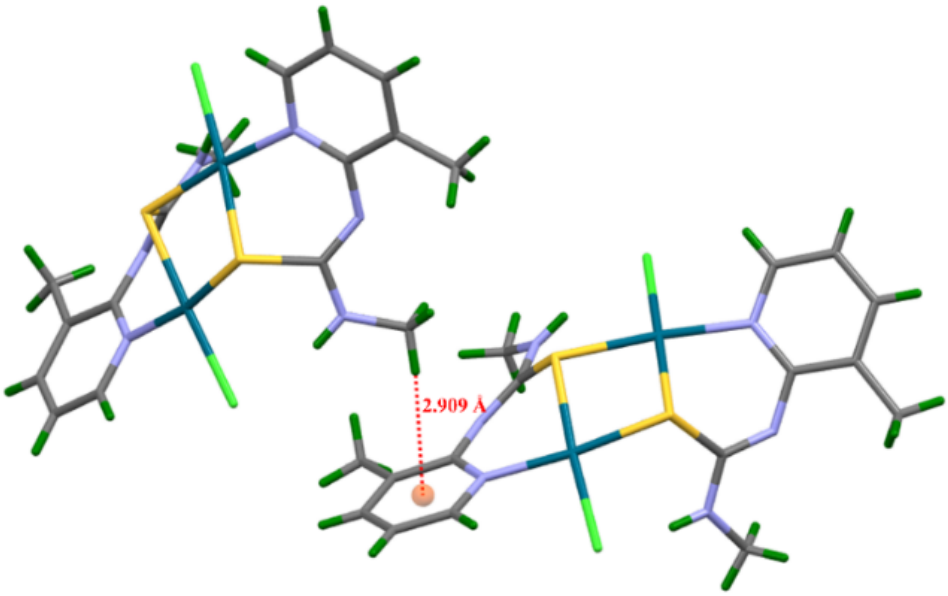

Supporting Fig. S19: Showing C-H···π (2.909 Å) hydrogen bonding interactions in **[Pd(M3MPyThU)Cl]$_2$**

10. Solution stability figure

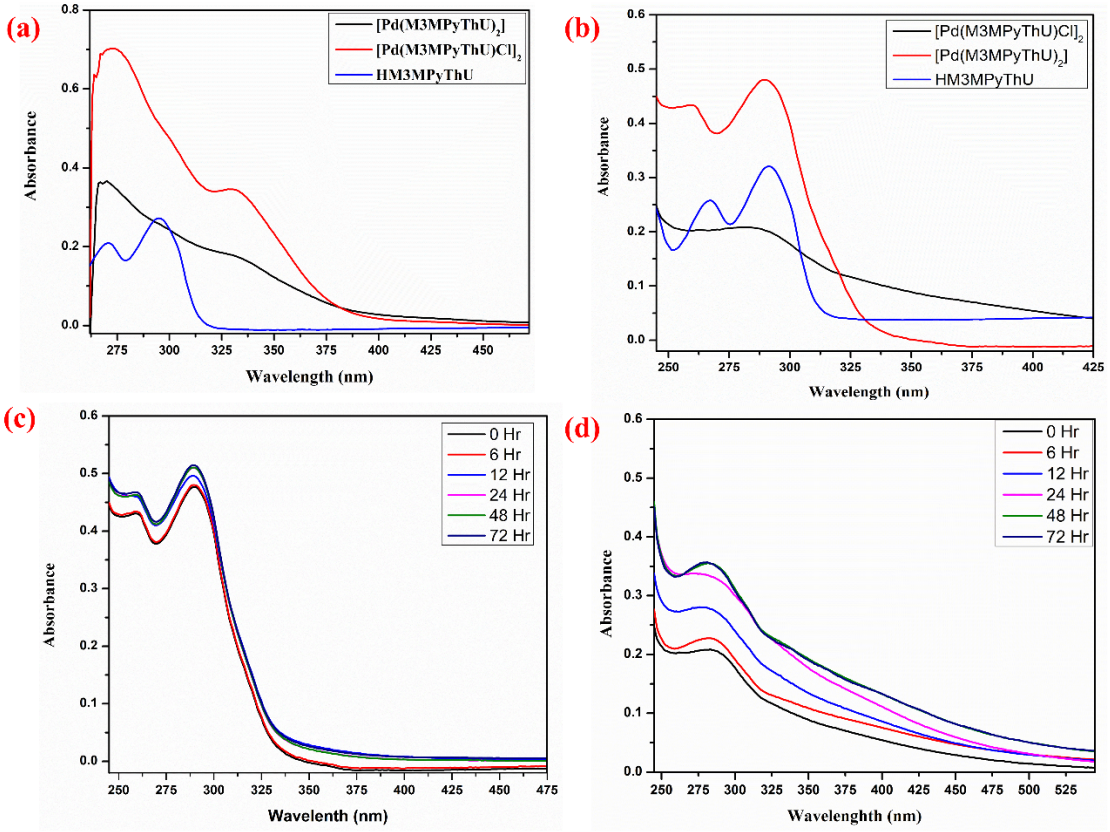

Supporting Fig. S20: Showing the UV-Vis spectra of compounds (10 µM) (a) in DMSO (b) in 1% DMSO/PBS (pH 7.4) and depicting the solution stability of complexes in 1% DMSO/PBS (pH 7.4) (c) **[Pd(M3MPyThU)]$_2$** (d) **[Pd(M3MPyThU)Cl]$_2$**

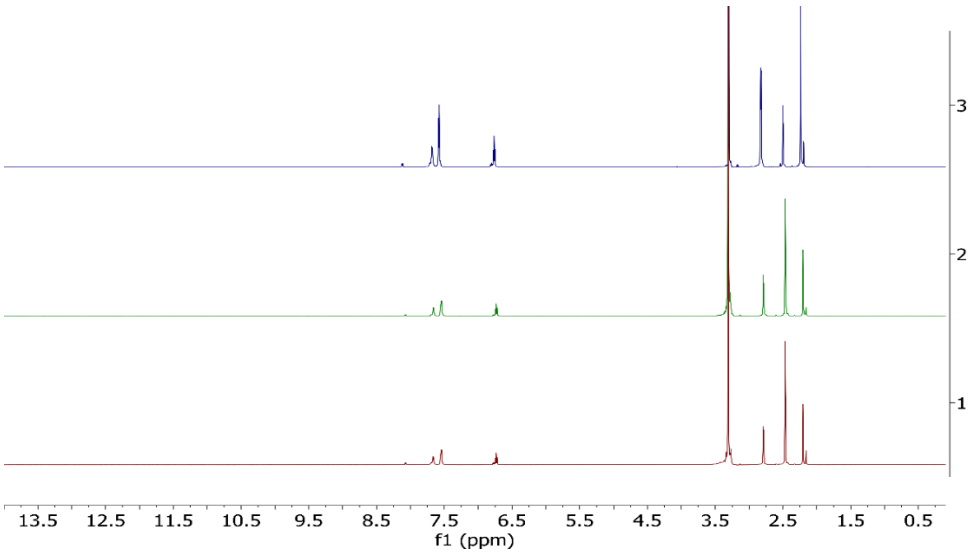

Supporting Fig. S21: Depicting the stability of **[Pd(M3MPyThU)$_2$]** through ^{1}H NMR spectra recorded over a period of 72 Hr (3:Blue 0 hr, 2:Green 24 Hr, 1:Red 72Hrs) in the presence of excess water peak around δ 3.33 ppm in dmso-D_6 peak at δ 2.50 ppm. Peaks around 2.25 and 2.82 ppm are due to two methyl groups, the proton in the aromatic region (δ 6.75-7,75 ppm) is due to the pyridine ring. No Significant changes has been observed in ^{1}H NMR spectra in the presence of water.

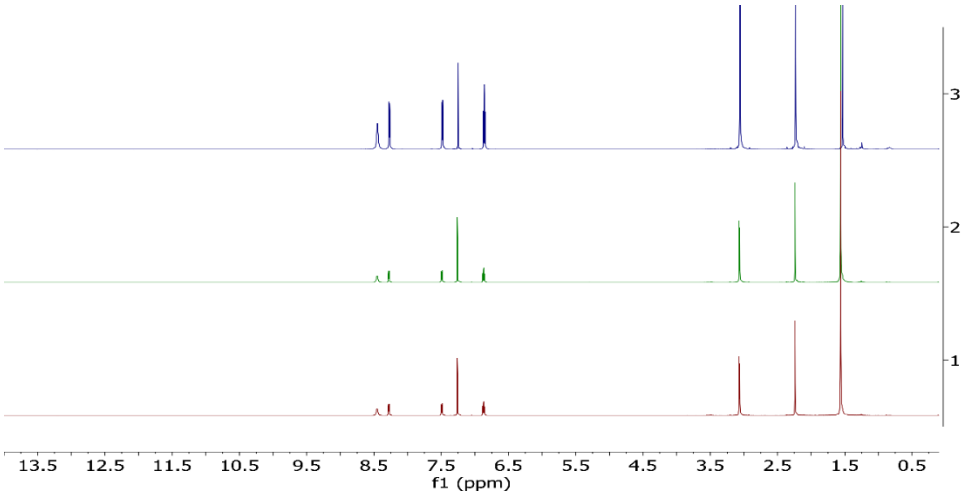

Supporting Fig. S22: Depicting the stability of **[Pd(M3MPyThU)Cl]$_2$** through ^{1}H NMR spectra recorded over a period of 72 Hr (3: Blue 0 hr, 2: Green 24 Hr, 1: Red 72Hr) in the presence of excess water peak around δ 1.56 ppm in $CDCl_3$ peak at δ 7.26 ppm. Peak around 2.25 and 3.06 ppm are due to two methyl groups, proton is aromatic region are due to pyridine ring (δ 6.75-8.50 ppm). No Significant changes has been observed in ^{1}H NMR spectra in presence of water.

11. Structure of complexes used in comparison

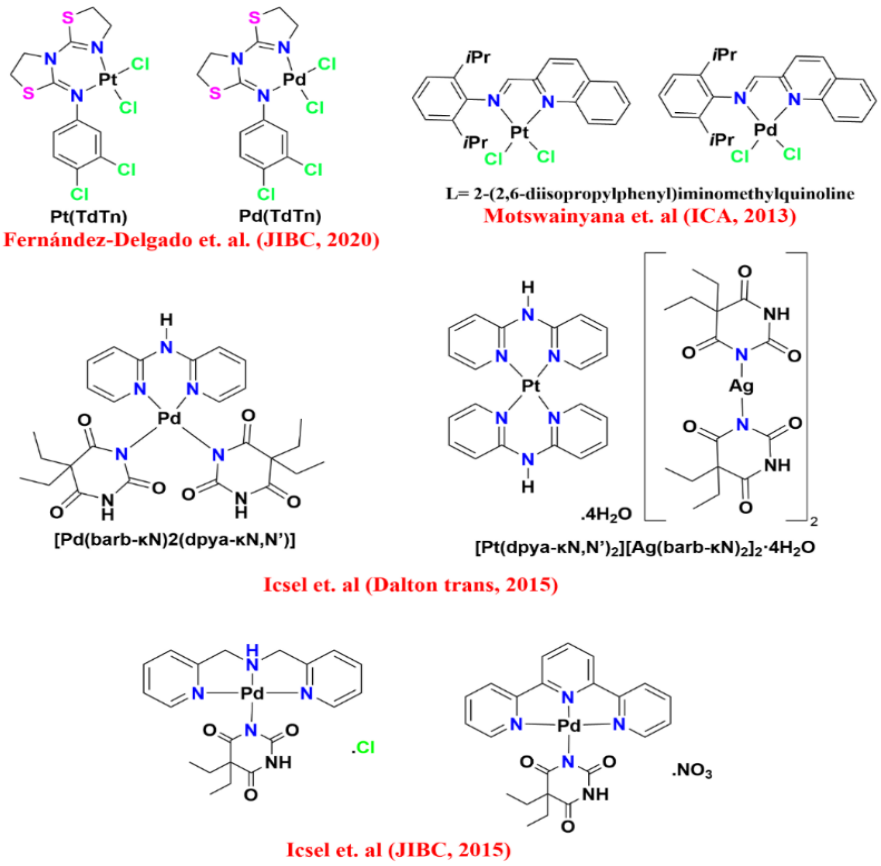

Supporting Fig. 23: Structures of previously reported complexes used in comparison study.[10-13]

12. References

1. O. V. Dolomanov, L. J. Bourhis, R.J. Gildea, J. A. K. Howard, H. Puschmann, OLEX2: a complete structure solution, refinement, and analysis program, *J. Appl. Crystallogr.* **2009**, 42, 339–341; https://doi.org/10.1107/s0021889808042726
2. G. M. Sheldrick, **SHELXL-2018** (2018) Program for Crystal Structure Refinement. University of Gottingen, Gottingen.
3. I. Usón, G. M. Sheldrick, An introduction to experimental phasing of macromolecules illustrated by SHELX; new autotracing features, *Acta Crysta Section D*: *Structural Biology*, **2018**, 74(2), 106-16. https://doi.org/10.1107/S2059798317015121
4. C. F. Macrae, P. R. Edgington, P. McCabe, E. Pidcock, G. P. Shields, R. Taylor, M. Towler, J. V. Streek, Mercury: visualization and analysis of crystal structures. Journal

of applied crystallography, **2006**, 39(3), 453-7. https://doi.org/10.1107/S002188980600731X

5. S. A. Elsayed, H. E. Badr, A. di Biase, A. M. El-Hendawy, Synthesis, characterization of ruthenium (II), nickel (II), palladium (II), and platinum (II) triphenylphosphine-based complexes bearing an ONS-donor chelating agent: Interaction with biomolecules, antioxidant, in vitro cytotoxic, apoptotic activity and cell cycle analysis. *J Inorg Biochem*, **2021**, 223, 111549. https://doi.org/10.1016/j.jinorgbio.2021.111549
6. P. Kumar, A. Nagarajan, P. D. Uchil, Analysis of cell viability by the MTT assay, *Cold spring harb protoc*, **2018**, 6. https://doi.org/10.1101/pdb.prot095505
7. D. Ribble, N. B. Goldstein, D. A. Norris, Y. G. Shellman, A simple technique for quantifying apoptosis in 96-well plates. *BMC Biotechnol*, **2005**, 5(12), 1-7. https://doi.org/10.1186/1472-6750-5-12
8. H. Kim, X. Xue, Detection of total reactive oxygen species in adherent cells by 2', 7'-dichlorodihydrofluorescein diacetate staining, *J Vis Exp.* **2020**, 23(160), e60682. https://doi.org/10.3791/60682
9. R. K. Singh, P. K. Verma, A. Kumar, S. Kumar, A. Acharya, Achyranthes aspera L. leaf extract induced anticancer effects on Dalton's Lymphoma via regulation of PKCα signaling pathway and mitochondrial apoptosis. *J Ethnopharmacol,* 2021, **274**, 22, 114060. https://doi.org/10.1016/j.jep.2021.114060
10. C. Icsel, V. T. Yilmaz, Y. Kaya, S. Durmus, M. Sarimahmut, O. Buyukgungor and E. Ulukaya, Cationic Pd(II)/Pt(II) 5,5-diethylbarbiturate complexes with bis(2-pyridylmethyl)amine and terpyridine: Synthesis, structures,DNA/BSA interactions, intracellular distribution, cytotoxic activity and induction of apoptosis, *J Inorg Biochem*, 2015, **152**, 38–52. https://doi.org/10.1016/j.jinorgbio.2015.08.026
11. W. M. Motswainyana, M. O. Onani, A. M. Madiehe, M. Saibu, J. Jacobs and L. Van Meervelt, Imino-quinolyl palladium(II) and platinum(II) complexes: Synthesis, characterisation, molecular structures and cytotoxic effect, *Inorg Chim Acta*, 2013, **400**, 197–202. https://doi.org/10.1016/j.ica.2013.02.029
12. C. Icsel, V. T. Yilmaz, Y. Kaya, H. Samli, W. T. A. Harrison and O. Buyukgungor, New palladium(II) and platinum(II) 5,5-diethylbarbiturate complexes with 2-phenylpyridine, 2,2’-bipyridine and 2,2’-dipyridylamine: synthesis, structures, DNA binding, molecular docking, cellular uptake, anti-oxidant activity and cytotoxicity, *Dalton Trans*, 2015, **44**, 6880–6895. https://doi.org/10.1039/C5DT00728C

13. E. Fernández-Delgado, F. de la Cruz-Martínez, C. Galán, L. Franco, J. Espino, E. Viñuelas-Zahínos, F. Luna-Giles and I. Bejarano, Pt(II) and Pd(II) complexes with a thiazoline derivative ligand: Synthesis, structural characterisation, antiproliferative activity and evaluation of proapoptotic ability in tumor cell lines HT-29 and U-937, *J Inorg Biochem*, 2020, **202**, 110870. https://doi.org/10.1016/j.jinorgbio.2019.110870